Current-driven dynamics of coupled domain walls in a synthetic antiferromagnet

Henri Saarikoski,[1] Hiroshi Kohno,[2] Christopher H. Marrows,[3] and Gen Tatara[1]
[1]*RIKEN Center for Emergent Matter Science (CEMS), 2-1 Hirosawa, Wako, Saitama 351-0198, Japan*
[2]*Department of Physics, Nagoya University, Nagoya 464-8602, Japan*
[3]*School of Physics and Astronomy, University of Leeds, Leeds LS2 9JT, United Kingdom*
(Received 22 July 2014; published 17 September 2014)

We develop the theory of magnetic domain-wall motion in coupled double-layer systems where electrons can hop between the layers, giving rise to an antiferromagnetic coupling. We demonstrate that the force from the interlayer coupling drives the walls and the effect of the extrinsic pinning is greatly reduced if the domain walls are initially separated. The threshold current density for metastable spin-aligned configurations is also much lower. We conclude that the interlayer coupling has a significant effect on domain-wall mobility in double-layer systems.

DOI: 10.1103/PhysRevB.90.094411 PACS number(s): 75.60.Ch, 75.78.Fg, 85.75.−d

I. INTRODUCTION

Domain walls in ferromagnetic materials involve magnetization reversal in a thin layer. The thickness of this layer is determined by the magnetic anisotropy energy and the exchange energy. Domain walls separate areas of different magnetization orientations and they are controllable using currents which create a spin torque that drives the wall. Therefore, devices using domain-wall dynamics hold promise for future high-speed, high-density, and nonvolatile data storage [1].

However, domain-wall motion is restricted by intrinsic and extrinsic pinning effects and current densities needed to move domain walls are typically high, of the order of 1×10^{12} A/m^2. The intrinsic pinning is due to the hard-axis magnetic anisotropy [2]. The extrinsic pinning involves, e.g., defects in individual layers [3]. Theoretically, it was demonstrated that in the adiabatic limit, where the wall is driven solely by the spin-transfer torque, the wall has to overcome the energy barrier arising from the hard-axis anisotropy energy, and that the wall is intrinsically pinned [2]. This energy barrier involves a threshold current below which a domain wall does not move or motion stalls soon after the current is turned on. In most cases, the threshold current of the intrinsic pinning is high [3]. The intrinsic pinning effect was observed in a perpendicularly magnetized Co-Ni nanowire with reduced hard-axis anisotropy [4]. The threshold current density was 2.5×10^{11} A/m^2 and it was insensitive to the applied magnetic field which was consistent with theoretical predictions [2]. Spin relaxation results in a torque orthogonal to the spin-transfer torque, and this torque, called the nonadiabatic torque, removes the intrinsic pinning effect and the threshold current is reduced [3,5,6]. The threshold current is then determined by the extrinsic pinning potential and the nonadiabaticity parameter, β. In principle, the intrinsic pinning effect can be removed by fabricating a wire which has a cross section of a perfect circle [7]. However, most of the experiments have been carried out in the regime where extrinsic pinning effects dominate [8].

For realizing fast domain-wall motion and low threshold current density, several experimental attempts have been carried out. Lepadatu *et al.* controlled the value of the nonadiabaticity parameter, β, by doping permalloy with vanadium [9]. They showed that V doping of 10% leads to an increase of β by a factor of about 2, but the threshold current did not improve since the spin polarization of the current was reduced by doping. On the other hand, doping with Gd also increases β, in this case leading to a slight reduction in threshold depinning current [10]. Trilayer Pt/Co/MgO structures were studied by Miron *et al.* [11,12]. They were motivated by the idea that Rashba spin-orbit interaction would emerge in interfaces of layers of insulators and metals in the presence of heavy atoms with strong spin-orbit interaction. This interaction would realize very efficient wall motion since it acts as a large β as predicted theoretically [13,14]. The wall velocity in that trilayer system was 400 m/s, which is two orders of magnitude larger than in single-layer systems, at current density of 3×10^{12} A/m^2 [12]. However, it turned out that the mechanism for fast wall motion was not due to the Rashba interaction. In fact, systematic analysis on Pt/CoFe/MgO and Ta/CoFe/MgO structures indicated that the spin Hall effect in Pt and Ta layers injects spin current into the ferromagnetic layer and induces a substantial torque on the domain wall, resulting in fast motion [15,16]. Due to high domain-wall velocities, artificial multilayered structures are promising for designing devices with efficient domain-wall motion. For lowering the threshold of the wall motion, coupled ferromagnets are useful. Magnetic field-driven depinning of domain walls in coupled nanostrips was studied using micromagnetic simulations in Ref. [17]. The coupling between the walls in the two adjacent wires is due to the magnetostatic coupling, and it was found that the depinning from notches is strongly affected by the coupling. The importance of the domain-wall type and the initial chirality of the two walls on the depinning was also reported, since these affect the strength of the magnetostatic coupling between the walls.

Here we develop theory of current-driven domain-wall motion in coupled double-layer systems where electrons can hop between the layers, giving rise to an antiferromagnetic coupling. The presence of antiferromagnetic coupling between the layers was demonstrated [18] for ultrathin films in the mid-1980s and it is used in applications such as magnetic stabilization of magnetoresistive recording heads [19]. The interlayer coupling induces an attractive force between the walls in the two different layers, and this force is expected to help depin the wall since the current drives both walls. We

derive equations of motion for the system in the presence of force from the interlayer coupling and calculate domain-wall dynamics from the resulting equations. It turns out that interlayer coupling indeed reduces the threshold current greatly if domain walls are initially separated at different pinning sites. The coupled-layer systems are therefore promising for efficient domain-wall motion not affected by localized random defects.

II. THEORETICAL MODEL

In this section we derive the equation of motion for domain walls in a ferromagnetic double-layer system. We label the layers by $i = 1,2$. The localized spin direction at position $\boldsymbol{r}$ and time t in each ferromagnetic layer is denoted by a unit vector field, $\boldsymbol{n}^{(i)}(\boldsymbol{r},t)$. We define a coordinate system such that the wire lies in the x-z plane, extended along the z direction, with the two layers stacked above each other in the y direction [see Fig. 1(a)]. The magnetic easy axis is along the z direction and the y direction is the magnetic hard axis. The spin Hamiltonian can then be written as

$$H_S = \sum_{i=1,2} \int_{V_i} \frac{d^3r}{a^3} \left[\left(\frac{JS^2}{2} \nabla \boldsymbol{n}^{(i)} \right)^2 - \frac{KS^2}{2} \left(n_z^{(i)}\right)^2 + \frac{K_\perp S^2}{2} \left(n_y^{(i)}\right)^2 \right], \quad (1)$$

where J, K, and $K_\perp$ are the strength of the exchange interaction, the easy-axis anisotropy energy, and the hard-axis anisotropy energy, respectively. In nanowires made from magnetically soft permalloylike materials, these anisotropy constants arise from shape anisotropy. The magnitude of spin is S, a is a lattice constant, and V_i denotes the volume of the ferromagnet i. We consider the case in which material constants are the same for both ferromagnets.

Coupling between the two ferromagnets is mediated by electron hopping between the layers. The in-plane component of the coupling is here antiferromagnetic, $\Delta_\parallel \geqslant 0$. We assume for generality that the out-of-plane component of the interlayer coupling $\Delta_\perp$ is different from the in-plane component, since this coupling is affected by the demagnetization field. Therefore, we consider here both antiferromagnetic ($\Delta_\perp > 0$) and ferromagnetic ($\Delta_\perp < 0$) out-of-plane couplings. We assume that the two ferromagnets are thin (compared with the domain-wall thickness) and that the interlayer coupling acts uniformly on the whole spin. The interlayer coupling is thus represented by the Hamiltonian

$$H_I = \int_{V_1} \frac{d^3r_1}{a^3} \int_{V_2} \frac{d^3r_2}{a^3} \left[\Delta_\parallel S^2 \left(n_x^{(1)}(\boldsymbol{r}_1) n_x^{(2)}(\boldsymbol{r}_2) + n_z^{(1)}(\boldsymbol{r}_1) n_z^{(2)}(\boldsymbol{r}_2) \right) + \Delta_\perp S^2 n_y^{(1)}(\boldsymbol{r}_1) n_y^{(2)}(\boldsymbol{r}_2) \right]. \quad (2)$$

Magnetic anisotropy is very common in thin ferromagnetic films. Therefore, we consider only Néel-type domain walls which have the domain-wall solution

$$\boldsymbol{n}^{(i)} = \begin{pmatrix} \sin\theta_i \cos\phi_i \\ \sin\theta_i \sin\phi_i \\ \cos\theta_i \end{pmatrix}, \quad (3)$$

where

$$\cos\theta_i = (-)^i \tanh \frac{z - Z_i(t)}{\lambda} \quad (4)$$

and $\sin\theta_i = [\cosh \frac{z-Z_i(t)}{\lambda}]^{-1}$, where θ is the angle between the moment and the z axis and $\phi_i(t)$ is the azimuthal angle around that axis and represents the out-of-plane angle of the spin in Fig. 1(b). The wall position is denoted by Z_i and λ is the thickness of the wall, given by $\lambda = \sqrt{J/K}$. The topological charge of the domain wall, given by the sign in Eq. (4), differs for the two domain walls as a result of the antiferromagnetic in-plane coupling. This property is essential in the dynamics of the system of coupled walls. The geometry of the synthetic antiferromagnet under consideration is shown in Fig. 1.

Current applied in the direction of the wire gives rise to two important effects: the adiabatic spin-transfer torque effect, which induces a torque on the domain wall, and a nonadiabatic contribution which is described as a force on the wall. The adiabatic effect is given by the spin-transfer Hamiltonian,

$$H_{ST} = -\sum_{i=1,2} \int_{V_i} \frac{d^3r}{a^3} \hbar S \frac{Pa^3}{2eS} (\boldsymbol{j} \cdot \nabla)\phi_i(\cos\theta_i - 1), \quad (5)$$

where $\boldsymbol{j}$ is the electric current density, $e(<0)$ is the electron charge, and P is the spin polarization of the current. The nonadiabatic contribution as well as damping are inserted later in the equations of motion.

By collecting all the above contributions we obtain the Lagrangian of the coupled double-layer system under applied current,

$$L = \sum_{i=1,2} \int_{V_i} \frac{d^3r}{a^3} \hbar S \dot{\phi}_i(\cos\theta_i - 1) - H_S - H_I - H_{ST}, \quad (6)$$

where the first term is the spin Berry phase term. We rewrite the Lagrangian in terms of the collective coordinates for the two walls, $Z_i(t)$ and $\phi_i(t)$ [see Fig. 1(b)]. The spin Berry phase

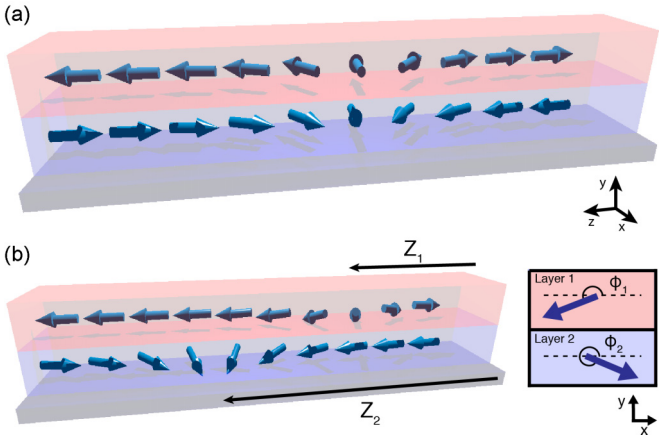

FIG. 1. (Color online) (a) Ground-state geometry of Néel-type domain walls in a synthetic double-layer antiferromagnet. (b) Coupling between the layers gives rise to an attractive force between the walls at finite separation $Z_1 - Z_2$. The figure shows a spin configuration which has out-of-plane angles $\phi_{1,2}$. Spin orientations at the center of the walls are shown in the inset.

term reduces to

$$\sum_{i=1,2}\int_{V_i}\frac{d^3r}{a^3}\hbar S\dot{\phi}_i(\cos\theta_i-1)=\sum_{i=1,2}\hbar N_i S(-)^i\phi_i\dot{Z}_i, \quad (7)$$

where $N_i\equiv\frac{2\lambda A_i}{a^3}$ is the number of spins in the wall, A_i is the cross-sectional area of the wire, and we used the fact that $\dot{\phi}_i\cos\theta_i$ is equivalent to $-\phi_i\frac{d}{dt}\cos\theta_i$ using integration by parts. One can easily show that

$$H_S=\sum_{i=1,2}N_iS^2\frac{K_\perp}{2}\sin^2\phi_i, \quad (8)$$

and

$$\begin{aligned}H_{\rm I}=&N_{\rm I}S[\Delta_\parallel u((Z_1-Z_2)/2)\cos\phi_1\cos\phi_2\\&+\Delta_\perp u((Z_1-Z_2)/2)\sin\phi_1\sin\phi_2\\&+\Delta_\parallel w((Z_1-Z_2)/2)],\end{aligned} \quad (9)$$

where $N_{\rm I}$ is the effective number of spins and

$$u(Z)\equiv\int_{-\infty}^{\infty}dz\frac{1}{\cosh z\cosh(z-2Z)}=2Z\,\mathrm{csch}(Z), \quad (10)$$

$$w(Z)\equiv\int_{-\infty}^{\infty}dz(1-\tanh z\tanh(z-2Z))=2Z\coth(Z). \quad (11)$$

The potentials $u(Z)$, $w(Z)$ and their derivatives are plotted in Fig. 2. After these calculations the Lagrangian reads

$$\begin{aligned}L=&\sum_{i=1,2}\hbar N_iS\left[(-)^i\frac{\phi_i}{\lambda}(\dot{Z}_i-v_e)-v_c\sin^2\phi_i\right]\\&-\hbar N_{\rm I}S[\Delta_\parallel u((Z_1-Z_2)/2)\cos\phi_1\cos\phi_2\\&+\Delta_\perp u((Z_1-Z_2)/2)\sin\phi_1\sin\phi_2\\&+\Delta_\parallel w((Z_1-Z_2)/2)],\end{aligned} \quad (12)$$

where $v_c\equiv\frac{K_\perp\lambda S}{2\hbar}$ and $v_e\equiv\frac{Pa^3}{2eS}j$.

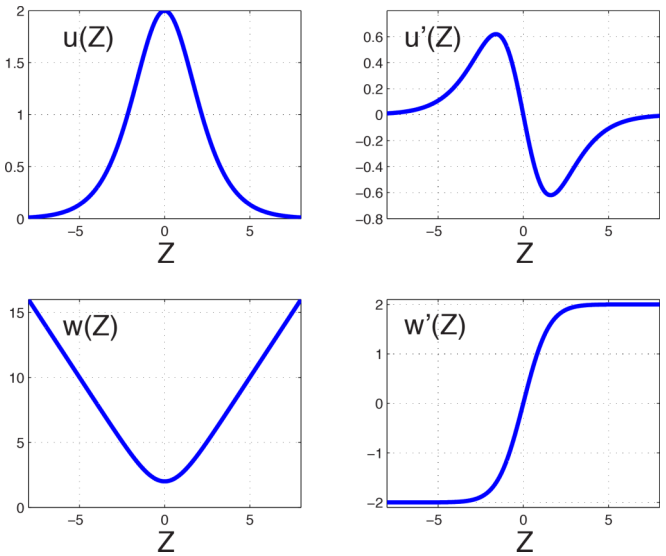

FIG. 2. (Color online) Potentials $u(Z)$ and $w(Z)$ and their derivatives, $u'(Z)$ and $w'(Z)$.

Now we include the effect of damping and nonadiabatic contribution of the current. The damping [20] is included as $\frac{\delta L}{\delta\dot{Z}_i}=\alpha\hbar N_iS\frac{\dot{Z}_i}{\lambda}$ and $\frac{\delta L}{\delta\dot{\phi}_i}=\alpha\hbar N_iS\dot{\phi}_i$. The nonadiabatic torque, represented by a parameter β, induces a force $\frac{\hbar N_ia^3}{2eS\lambda^2}\beta Pj$. Since $L=-\hbar N_1S\frac{\phi_1}{\lambda}\dot{Z}_1+\hbar N_2S\frac{\phi_2}{\lambda}\dot{Z}_2-H$, the equations of motion obtained by differentiating with respect to Z_1 and Z_2 are

$$-\hbar N_1S\frac{\dot{\phi}_1}{\lambda}=F_1,\quad \hbar N_2S\frac{\dot{\phi}_1}{\lambda}=F_2, \quad (13)$$

where

$$\begin{aligned}F_1\equiv&-\frac{\delta H}{\delta Z_1}-\alpha\hbar N_1S\frac{\dot{Z}_i}{\lambda}+\frac{\hbar N_1a^3}{2eS\lambda^2}\beta Pj,\\F_2\equiv&-\frac{\delta H}{\delta Z_2}-\alpha\hbar N_2S\frac{\dot{Z}_i}{\lambda}+\frac{\hbar N_2a^3}{2eS\lambda^2}\beta Pj,\end{aligned} \quad (14)$$

are the forces. The equations of motion thus read

$$\begin{aligned}-\dot{Z}_1-\alpha\lambda\dot{\phi}_1=&v_c\sin2\phi_1-v_e-\mu_1u((Z_1-Z_2)/2)\\&\times(\Delta_+\sin(\phi_1-\phi_2)+\Delta_-\sin(\phi_1+\phi_2)),\end{aligned} \quad (15)$$

$$\begin{aligned}\dot{\phi}_1-\alpha\frac{\dot{Z}_1}{\lambda}=&-\frac{\beta}{\lambda}v_e+\frac{\mu_1}{2}[\Delta_\parallel w'((Z_1-Z_2)/2)\\&+u'((Z_1-Z_2)/2)(\Delta_+\cos(\phi_1-\phi_2)\\&+\Delta_-\cos(\phi_1+\phi_2))],\end{aligned} \quad (16)$$

$$\begin{aligned}\dot{Z}_2-\alpha\lambda\dot{\phi}_2=&v_c\sin2\phi_2+v_e\\&+\mu_2u((Z_1-Z_2)/2)(\Delta_+\sin(\phi_1-\phi_2)\\&-\Delta_-\sin(\phi_1+\phi_2)),\end{aligned} \quad (17)$$

$$\begin{aligned}-\dot{\phi}_2-\alpha\frac{\dot{Z}_2}{\lambda}=&-\frac{\beta}{\lambda}v_e-\frac{\mu_2}{2}[\Delta_\parallel w'((Z_1-Z_2)/2)\\&+u'((Z_1-Z_2)/2)(\Delta_+\cos(\phi_1-\phi_2)\\&+\Delta_-\cos(\phi_1+\phi_2))],\end{aligned} \quad (18)$$

where $\Delta_\pm\equiv\frac{1}{2}(\Delta_\parallel\pm\Delta_\perp)$ and $\mu_i\equiv N_1/N_i$. The μ_i parameters of the planes determine whether the system is a balanced synthetic antiferromagnet at $\mu_1=\mu_2$ or an unbalanced synthetic ferrimagnet at $\mu_1\neq\mu_2$.

III. EFFECT OF PINNING

Domain-wall dynamics is affected by impurities, notches, and other nonuniformities in the layers. We model such nonuniformities using pinning forces on the domain walls. We are interested in calculating the terminal velocity of the domain walls under applied current when the domain walls are initially pinned in both layers. We consider, therefore, one pinning potential in each layer at distance ℓ from each other [20]:

$$F=-k_0^{(1)}(Z_1-\ell)\theta(\xi-|Z_1-\ell|)-k_0^{(2)}Z_2\theta(\xi-|Z_2|), \quad (19)$$

where $k_0^{(i)}$ $(i=1,2)$ are constants representing the strength of the potentials, ξ is the width of the potential, and $\theta(x)$ is a step function. We set the potential width ξ in both layers. Using

$k_i \equiv \frac{\lambda}{\hbar N_i S} k_0^{(i)}$, defining center of mass Z_+ and the difference Z_- in the domain-wall positions using $Z_\pm \equiv \frac{1}{2}(Z_1 \pm Z_2)$ as well as the average phase ϕ_+ and the difference in the phase using $\phi_\pm \equiv \frac{1}{2}(\phi_1 \pm \phi_2)$, and denoting $\mu_\pm = (\mu_1 \pm \mu_2)/2$ we obtain the final equations for motion:

$$\dot{Z}_+ + \alpha\lambda\dot{\phi}_- = -\nu_c \cos 2\phi_+ \sin 2\phi_- + \nu_e + u(Z_-)(\mu_+\Delta_+ \sin(2\phi_-) + \mu_-\Delta_- \sin(2\phi_+)), \tag{20}$$

$$\dot{\phi}_- - \alpha\frac{\dot{Z}_+}{\lambda} = \frac{k_1}{2}(Z_+ + Z_- - \ell)\theta(\xi - |Z_+ + Z_- - \ell|) + \frac{k_2}{2}(Z_+ - Z_-)\theta(\xi - |Z_+ - Z_-|) - \frac{\beta}{\lambda}\nu_e + \frac{\mu_-}{2}[\Delta_\parallel w'(Z_-) + u'(Z_-)(\Delta_+ \cos(2\phi_-) + \Delta_- \cos(2\phi_+))], \tag{21}$$

$$\dot{Z}_- + \alpha\lambda\dot{\phi}_+ = -\nu_c \sin 2\phi_+ \cos 2\phi_- + u(Z_-)(\mu_-\Delta_+ \sin(2\phi_-) + \mu_+\Delta_- \sin(2\phi_+)), \tag{22}$$

$$\dot{\phi}_+ - \alpha\frac{\dot{Z}_-}{\lambda} = \frac{k_1}{2}(Z_+ + Z_- - \ell)\theta(\xi - |Z_+ + Z_- - \ell|) - \frac{k_2}{2}(Z_+ - Z_-)\theta(\xi - |Z_+ - Z_-|) + \frac{\mu_+}{2} \times [\Delta_\parallel w'(Z_-) + u'(Z_-)(\Delta_+ \cos(2\phi_-) + \Delta_- \cos(2\phi_+))]. \tag{23}$$

IV. TERMINAL VELOCITY OF UNPINNED DOMAIN WALLS

In the absence of pinning potentials the terminal velocity of the domain wall can be analytically solved. We first assume that the domain-wall separation remains small, i.e., $|Z_-| \ll \lambda$, which gives approximately $u'(Z_-) = 0$ and $w'(Z_-) = 0$. We assume also that $\phi_\pm$ changes with time, resulting in vanishing of time averages of $\sin 2\phi_\pm$ and $\cos 2\phi_\pm$. After time averaging we see that the terminal velocities are not affected by the interlayer coupling:

$$\langle\dot{Z}_+\rangle = \frac{1}{1+\alpha^2}\nu_e(1+\alpha\beta), \quad \langle\dot{\phi}_-\rangle = \frac{1/\lambda}{1+\alpha^2}\nu_e(\alpha-\beta), \quad \langle\dot{Z}_-\rangle = 0, \quad \langle\dot{\phi}_+\rangle = 0. \tag{24}$$

We then assume that the separation of the domain wall grows with time, e.g., $|Z_-| \gg \lambda$. We can then approximate $u(Z_-) = u'(Z_-) = 0$ and $w'(Z_-) = 2\,\mathrm{sgn}(Z_-)$. After time averaging the terminal velocities are then

$$\langle\dot{Z}_+\rangle = \frac{1}{1+\alpha^2}[\nu_e(1+\alpha\beta) + \alpha\lambda\mu_-\Delta_\parallel \mathrm{sgn}(Z_-)], \quad \langle\dot{\phi}_-\rangle = \frac{1/\lambda}{1+\alpha^2}[\nu_e(\alpha-\beta) + \lambda\mu_-\Delta_\parallel \mathrm{sgn}(Z_-)], \quad \langle\dot{Z}_-\rangle = -\frac{1}{1+\alpha^2}\alpha\mu_+\Delta_\parallel \mathrm{sgn}(Z_-), \quad \langle\dot{\phi}_+\rangle = \frac{1/\lambda}{1+\alpha^2}\mu_+\Delta_\parallel \mathrm{sgn}(Z_-). \tag{25}$$

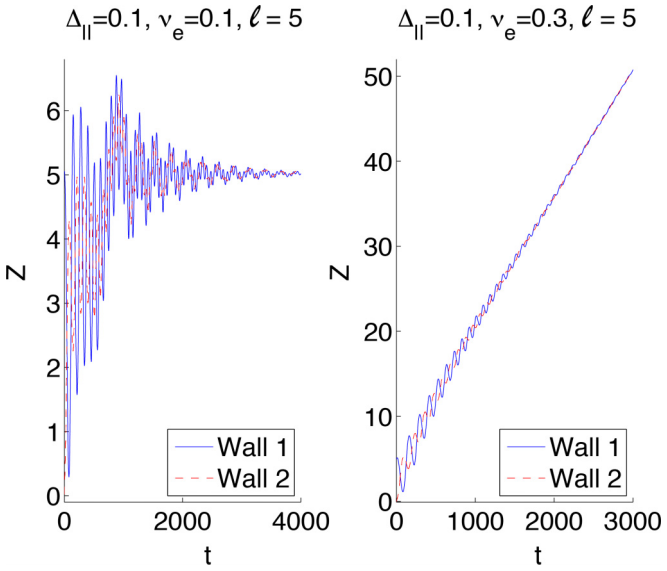

FIG. 3. (Color online) Motion of coupled domain walls in double-layer systems under extrinsic pinning. The current is switched on at time $t = 0$ and positions Z of the two domain walls in the system are calculated for pinning potentials which are located at $Z_1 = 5$ and at $Z_2 = 0$. When the current is insufficient to unpin the walls they oscillate in the pinning potentials with dampening amplitude (left). When the current is sufficiently large, it unpins the walls aided by the force from the interlayer coupling and the walls start moving (right). Eventually the walls move together with a vanishing phase difference. The terminal velocity is calculated from this limiting motion.

We see that in this limit the velocity increases with interlayer coupling. This can be understood from the antiferromagnetic coupling of the walls which exerts a force on the walls. In practice unpinned walls which are first at finite distance from each other move fast until the separation vanishes. Then the walls start moving together at a lower velocity determined by Eq. (24). This typical behavior is shown in numerical simulations in Fig. 3.

V. THRESHOLD CURRENT

Equations (20)–(23) are a group of first-order differential equations. We integrate the solution from initial conditions using a numerical Runge-Kutta-Fehlberg fourth-order method with a fifth-order error estimator for the adaptive step size. We use dimensionless units in calculations by fixing $\nu_c = 1$ and setting the thickness of the wall $\lambda = 1$. The time is measured in terms of a dimensionless quantity, $t\nu_c/\lambda = tK_\perp S/(2\hbar)$. We consider separately the adiabatic and nonadiabatic regimes. In the former regime adiabatic torque on the wall dominates dynamics and in the latter case the nonadiabatic force gives the most important contribution.

Due to the terms which depend on $Z_\pm$ and $\phi_\pm$ the time evolution of the system depends on the initial separation of the domain walls as well as the difference in their phases. A slight variation in the initial domain-wall positions and phases is introduced in order to simulate experimental situations at finite temperature and in order to avoid special limiting solutions to the differential equations, for instance when terms on the

right-hand side vanish at $\phi_+ = \phi_- = 0$. This also smooths out the effect of discontinuous external pinning potentials. We use tiny displacements to the initial domain-wall positions and phases using random numbers from a uniform distribution giving a ± 0.01 change in the wall position with respect to each other (in units of wall thickness, λ). The domain wall velocity is evaluated after a sufficiently long time when the domain-wall motion has stabilized.

The initial fluctuation of the wall position, δZ, corresponds to energy fluctuation of $\delta\mathcal{E} = \frac{k_0}{2}(\delta Z)^2 = NV_0(\delta Z/\xi)^2$, where the pinning potential depth per spin is $V_0 \equiv \frac{\hbar S}{2\lambda}k\xi^2$ (we suppress here the suffix $i = 1,2$ denoting the layer). In numerical calculations, the time is measured in terms of a dimensionless quantity, $tv_c/\lambda = tK_\perp S/(2\hbar)$, and thus a pinning strength $k = 0.1$ we use in the calculations would correspond to the pinning potential of $V_0/K_\perp = kS^2\xi^2/(4v_c) = 2.5 \times 10^{-2}$ if we choose $S \simeq 1$ and $\xi \simeq \lambda$. For permalloy wires, $K_\perp \sim 0.03 \sim 2.4$ K [21], and if we consider a wall with thickness of 100 nm in a wire of cross-sectional area of 400 nm $\times$ 5 nm, we have $N = 1.3 \times 10^7$ (for $a = 2.5$ Å) as the number of spins in the wall. The fluctuation energy for $\delta Z = 0.01$, therefore, is $\delta\mathcal{E} = 30K_\perp = 1$–$72$ K. The initial fluctuations of ± 0.01 in the calculations is therefore small in magnitude in comparison to those expected for permalloy wires at room temperature.

A. Extrinsic pinning

We insert pinning potentials in both layers as described in Sec. III. The initial conditions are chosen to fix the domain walls at the center of the pinning potentials. Details of the domain-wall dynamics depend now on the relative strength of the parameters in the model. At finite values of the nonadiabatic torque β the extrinsic pinning potentials usually restrict domain-wall motion and a large driving current is needed to unpin the walls. This limits the usefulness of magnetic domains in applications, and means to improve mobility have been the focus of intense research efforts.

Figure 3 shows typical domain-wall dynamics when the walls are pinned by the potentials and when the interlayer coupling is large enough to unpin the walls, respectively. If the force from the interlayer coupling [terms containing $\Delta_{||}$ or $\Delta_\perp$ in Eqs. (20)–(23)] is not sufficiently large to unpin the walls, the walls absorb the momentum, leading to oscillations. The threshold current is the current at which depinning occurs. The depinning process is clearly aided by the force from the separation of the domain walls and once the walls clear the pinning potentials they start to travel together with the difference in phases eventually vanishing. In this limit the velocity decreases as discussed in Sec. IV. We calculate domain-wall motion in the presence of pinning potentials from the velocity in this limit.

1. Weak nonadiabatic force ($\beta < \alpha$)

We focus first on the regime of weak force from the nonadiabatic torque β. We set $k_{1,2} = 0.1$, $\beta = 0.005$, and the damping term $\alpha = 0.01$. We set the potential well width $\xi = 1$, which is comparable in size to the domain-wall width. We find also that the potential well width does not significantly affect the results since the wall motion is coupled also inside very wide potential wells. The in-plane interlayer coupling is assumed to be antiferromagnetic ($\Delta_\parallel > 0$) and we first neglect the perpendicular component in the calculations, setting $\Delta_\perp = 0$. We investigate the effect of the perpendicular component later.

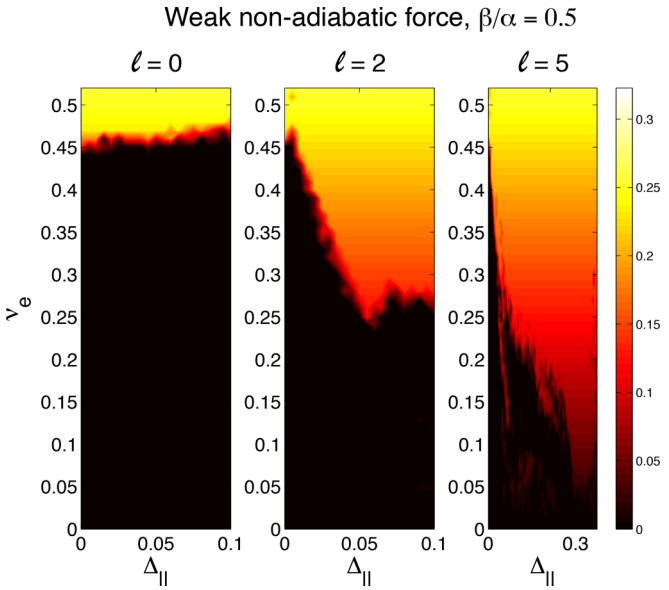

FIG. 4. (Color online) Averaged terminal domain-wall velocity (given by the color bar) in double-layer systems under weak nonadiabatic force ($\beta/\alpha = 0.5$). The velocity is calculated as a function of antiferromagnetic in-plane interlayer coupling $\Delta_{||}$ and velocity of driving electrons v_e. The thicknesses of the layers are $\mu_1 = 1$ and $\mu_2 = 1/2$. The velocities are calculated for different distances between the pinning potentials ℓ. The interlayer coupling helps unpin the domain walls and lowers the threshold current at $\ell > 0$. Note that the range for $\Delta_{||}$ is larger at $\ell = 5$.

Figure 4 shows terminal domain-wall velocity as a function of velocity of driving electrons v_e and strength of the in-plane interlayer coupling Δ at different distances between the pinning potential sites, ℓ. The velocity is calculated for asymmetric domain-wall configurations ($\mu_1 = 1$ and $\mu_2 = 1/2$).

We find that the threshold current for domain-wall motion decreases rapidly with increasing antiferromagnetic interlayer coupling at finite distance between the pinning potentials. The threshold current is lowered at large distances between the pinning potential sites. Assuming that impurities can be modeled using pinning potentials with a random distribution and no correlations between the layers, our results mean that interlayer coupling makes coupled domain walls in disordered systems much easier to depin with a current.

Our result can be qualitatively explained assuming that the separation between the walls is large and the wall in the first layer is outside of the pinning potential, i.e., $Z_1 \gg \xi$ and $w'(Z_-) \approx 2\,\mathrm{sgn}(Z_-)$ (see Fig. 2). We further assume that the angles $\phi_\pm$ change slowly and that the domain walls are separated so that $Z_1 > Z_2$. Subtracting Eq. (23) from Eq. (21) then gives

$$\frac{\alpha}{\lambda}\dot{Z}_2 = k_2 Z_2 - \frac{\beta}{\lambda}v_e - \mu_2\Delta_\parallel. \tag{26}$$

This shows that the coupling exerts a force on the domain wall which is proportional to $\Delta_\parallel$. The threshold current due to the extrinsic pinning potential is determined by the condition for vanishing of the total force. The wall is depinned when the force, the right-hand side of Eq. (26), vanishes at the highest pinning potential strength,

$$k_2\xi = \frac{\beta}{\lambda}v_e + \mu_2\Delta_\parallel. \quad (27)$$

The threshold value of the velocity of the driving electrons, v_e, is reduced in the presence of the coupling $\Delta_\parallel$. We note that $w'(Z_-)$ increases rapidly as a function of distance between the walls and saturates for large distances. Therefore, even a small displacement for one of the walls induces a force on the coupled wall and decreases the threshold current density. As a consequence large initial domain-wall separation assists the depinning process slightly and smooths out the sharp boundary between the regimes. In this crossover regime some initial domain-wall configurations lead to depinning of the walls. Finite temperature in experiments may therefore assist the depinning process. In the case of strong pinning potentials the threshold current has only a weak dependence on the pinning potential strength [20]. We find that even in this regime the interlayer coupling decreases the threshold current.

2. *Strong nonadiabatic force ($\beta \gg \alpha$)*

Next we consider the regime where β is large and the nonadiabatic torque predominates. The domain-wall motion is then driven by the force exerted by this torque. Threshold current density is low and the terminal domain-wall velocity above the threshold current is proportional to β/α [3]. In this regime mobility is high and the threshold current depends on the interlayer coupling and the distance between the pinning potential sites. Figure 5 shows terminal domain-wall velocity when the pinning potentials are located at different positions with respect to each other ($\ell = 0,1,2$). We find that the nonadiabatic force from the interlayer coupling drives the walls and the effect of the extrinsic pinning is greatly reduced at finite ℓ. In this regime the threshold current is strongly reduced by even a weak interlayer coupling.

At high driving currents ($v_e > 0.2$) and weak pinning strength the domain-wall mobility is reduced due to a mechanism which is analogous to the Walker breakdown in magnetic fields [22,23]. The combination of strong nonadiabatic driving and the interlayer coupling increases domain-wall mobility significantly at finite ℓ. We see a factor-of-5 improvement in the threshold current at the coupling strength $\Delta_\parallel = 0.1$. Otherwise, the behavior is similar to the case of weak nonadiabatic driving force and consistent with the analytical calculation in Sec. VA1.

So far we have neglected the out-of-plane component of the interlayer coupling $\Delta_\perp$. The out-of-plane component is affected by the demagnetization field and therefore it can differ from the in-plane coupling in experiments. However, calculations at fixed in-plane coupling strength $\Delta_\parallel = 0.5$ with ferromagnetic and antiferromagnetic out-of-plane coupling strength ($\Delta_\perp = +0.5$ and $\Delta_\perp = -0.5$, respectively) show little effect on the threshold current (Fig. 6). Antiferromagnetic out-of-plane coupling gives the highest domain-wall velocity close to the regime of Walker breakdown. We find also that the potential well width ξ does not significantly affect the results since the wall motion is coupled also inside very wide potential wells.

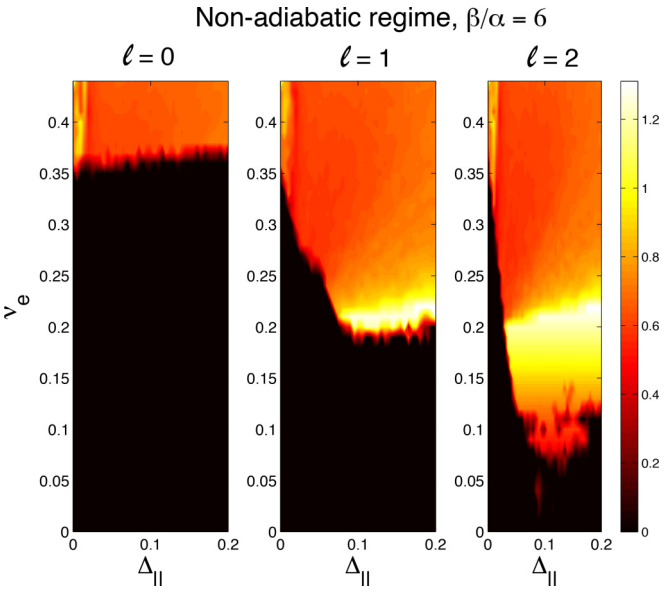

FIG. 5. (Color online) Averaged terminal domain-wall velocity (given by the color bar) in double-layer systems in the regime of strong nonadiabatic driving ($\beta/\alpha = 6$) and different distances between the pinning potential sites, ℓ. In this regime the unpinned domain-wall velocity is proportional to β/α until the point of Walker breakdown at $v_e \simeq 0.2$. In-plane interlayer coupling is antiferromagnetic ($\Delta = \Delta_\parallel > 0$) and improves domain-wall mobility at finite ℓ. The layers have unequal thickness $\mu_1 = 1$, $\mu_2 = 1/2$, and $\alpha = 0.01$.

3. *Evolution of metastable states*

Next we study metastable states corresponding to parallel spin alignment at the center of the walls ($\phi_1 = \phi_2 = 0$) [see

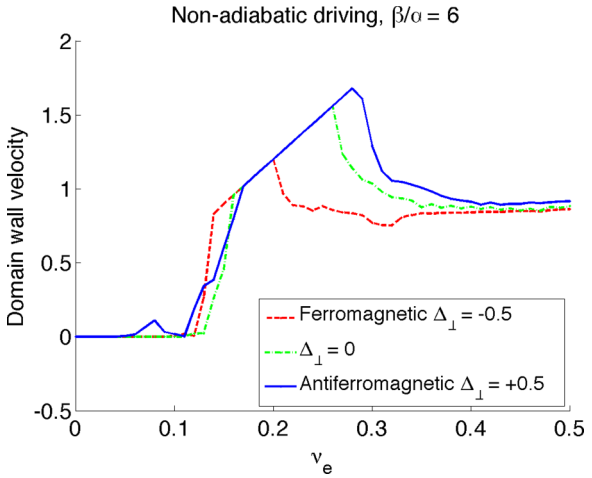

FIG. 6. (Color online) Averaged terminal domain-wall velocity in double-layer systems in the nonadiabatic driving regime with fixed in-plane coupling strength $\Delta_\parallel = +0.5$ and ferromagnetic ($\Delta_\perp = -0.5$), vanishing ($\Delta_\perp = 0$), and antiferromagnetic ($\Delta_\perp = +0.5$) out-of-plane component, respectively. Layer thickness $\mu_1 = 1$ and $\mu_2 = 0.5$. Distance between the pinning potential sites is $\ell = 2$.

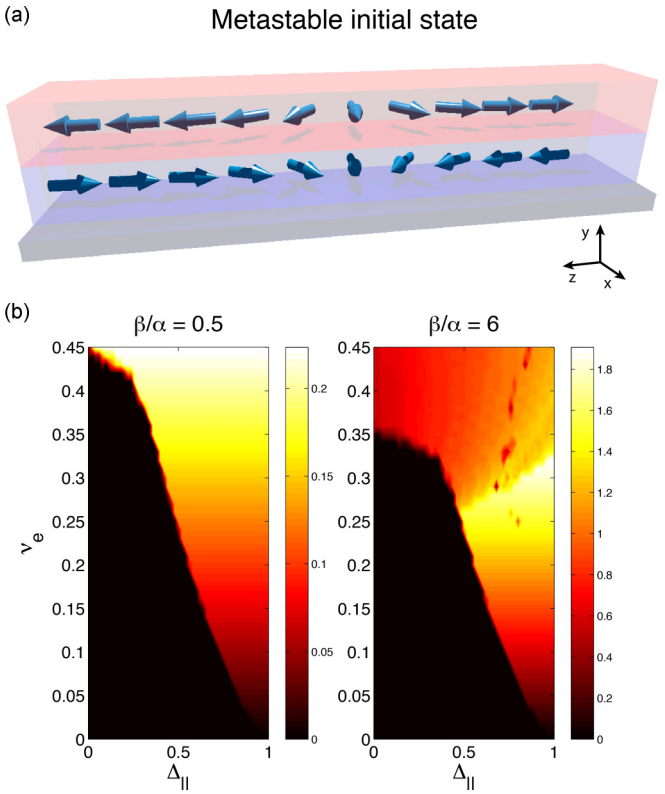

FIG. 7. (Color online) (a) A metastable initial state with parallel spin orientations at the center of the walls ($\phi_1 = \phi_2 = 0$). (b) Averaged terminal domain-wall velocity for the initial metastable states. The in-plane interlayer coupling is antiferromagnetic ($\Delta_{||} > 0$) and the out-of-plane component is $\Delta_\perp = 0$. Figure shows the regime of weak nonadiabatic force ($\beta/\alpha = 0.5$) and the regime of strong nonadiabatic driving ($\beta/\alpha = 6$). The threshold current decreases with increasing interlayer coupling in both cases. The layers have unequal thickness $\mu_1 = 1$, $\mu_2 = 1/2$, the pinning potential strength is $k_1 = k_2 = 0.1$, and the pinning sites are at the same position, $\ell = 0$.

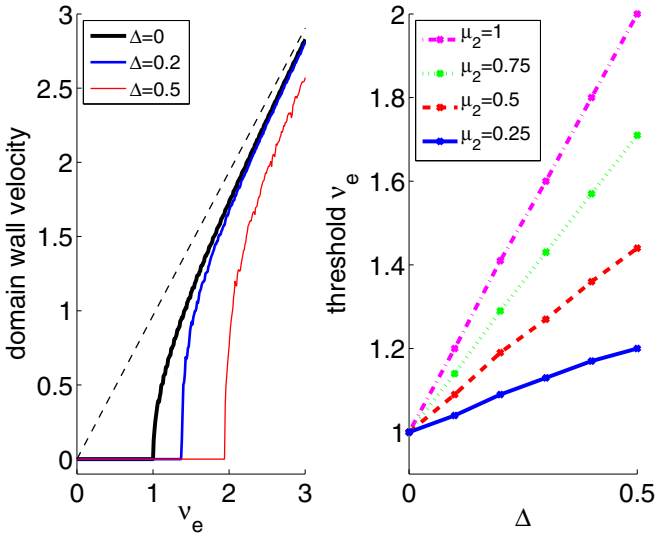

FIG. 8. (Color online) Terminal domain-wall velocity under intrinsic pinning in the absence of extrinsic pinning ($k_1 = k_2 = 0$). Interlayer coupling is assumed to be antiferromagnetic and isotropic, $\Delta_{||} = \Delta_\perp = \Delta$. The domain-wall velocity as a function of the velocity of driving electrons, v_e, at $\Delta = 0, 0.25$, and 0.5 at equal layer thickness $\mu_1 = \mu_2 = 1$ shown at left. The threshold v_e at different layer thicknesses μ_2 fixing $\mu_1 = 1$ shown at right.

Fig. 7(a)]. Energy associated with this initial spin alignment increases with interlayer coupling and helps depin the domain walls. Simulations show then that the system evolves until the final states have antiparallel spin alignment. The threshold current decreases strongly with the increasing interlayer coupling even at $\ell = 0$ in the regimes of both weak and strong nonadiabatic driving [Fig. 7(b)]. We find an order-of-magnitude difference in the threshold current density when the interlayer coupling strength is large.

B. Intrinsic pinning

In the case of adiabatic driving ($\beta \to 0$) the domain-wall dynamics is driven purely by the spin-transfer torque. The intrinsic pinning effects dominate domain-wall dynamics over extrinsic effects [2]. Intrinsic pinning is caused by the hard-axis magnetic anisotropy. We investigate here whether the interlayer coupling modifies the intrinsic pinning within our model at $\beta = 0$ assuming that there are no extrinsic pinning potentials $k_{1,2} = 0$. Figure 8 shows the domain-wall terminal velocity as a function of velocity of driving electrons at zero and finite interlayer coupling Δ. In the absence of interlayer coupling a high threshold current is needed to move the domain wall as discussed in Ref. [20]. The threshold current is attributed to the fact that a domain wall can absorb spin torque and deform instead of the torque setting the domain wall into motion. Calculations indicate that intrinsic pinning is stronger in the presence of interlayer coupling (Fig. 9). The domain-wall motion stalls after an initial boost from the spin torque of electron current and this effect increases with the strength of the interlayer coupling. The effect is largest for symmetric layers (Fig. 8). This effect is due to

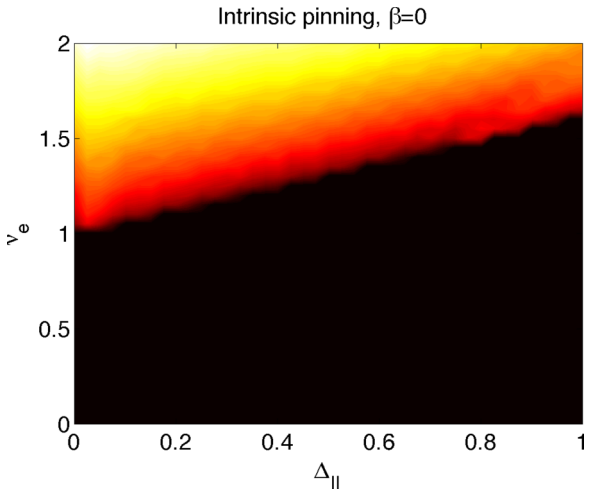

FIG. 9. (Color online) Averaged terminal domain-wall velocity under intrinsic pinning. Layers have unequal thickness $\mu_1 = 1$, $\mu_2 = 1/2$. In the absence of nonadiabatic torque the interlayer coupling moderately increases the threshold current needed to move the domain walls.

enhancement of the effective magnetic hard-axis anisotropy. The magnetic hard-axis anisotropy is proportional to ν_c. Close to the ground-state spin configuration $\phi_1 = 0$, $\phi_2 = \pi$; the $\Delta_\pm$-dependent terms in the equations of motion [Eqs. (15) and (17)] combine with the term which is proportional to ν_c and therefore the anisotropy is effectively higher.

VI. DISCUSSIONS

In our theory the force from the interlayer coupling facilitates significantly domain-wall motion in the regime where extrinsic pinning effects dominate. Even a low interlayer coupling improves mobility and in the limit of high interlayer coupling our theory predicts a much lower threshold current for the domain walls pinned at random impurity sites. A domain-wall separation which is of the order of the wall width is large enough to significantly improve domain-wall mobility. This effect is further expected to be enhanced at elevated temperatures due to thermal fluctuations in the domain-wall positions. In contrast to the extrinsic pinning regime, the interlayer coupling enhances effectively the hard-axis isotropy, giving rise to no mobility improvement in the regime where intrinsic pinning effects dominate.

We find that the depinning threshold depends strongly on the initial wall configuration as was discussed in the context of metastable spin-aligned states. This was also reported in the case of magnetostatically coupled walls driven by a magnetic field [17]. A magnetostatically repulsive interaction can reduce the depinning field. This bears some similarity to our results. However, an essential difference between the field-driven and current-driven cases is that head-to-head and tail-to-tail configurations are pushed in the same direction by the current but in opposite directions by a magnetic field.

We have shown theoretically that interlayer coupling improves domain-wall mobility in correlated bilayer systems. The interlayer coupling greatly reduces the effective pinning potential depth when the pinning potentials are uncorrelated in the two layers. Bilayer systems are thus promising candidates for realization of efficient domain-wall control with low current densities.

ACKNOWLEDGMENTS

We thank Serban Lepadatu for valuable comments and discussions. This work was supported by a Grant-in-Aid for Scientific Research (C) [Grants No. 25400344 (G.T.) and No. 26390014 (H.S.)] from the Japan Society for the Promotion of Science, UK-Japanese Collaboration on Current-Driven Domain Wall Dynamics from JST, and the EPSRC through Grant No. EP/J000337/1.

[1] M. Hayashi, L. Thomas, R. Moriya, C. Rettner, and S. S. P. Parkin, Science **320**, 209 (2008).
[2] G. Tatara and H. Kohno, Phys. Rev. Lett. **92**, 086601 (2004).
[3] A. Thiaville, Y. Nakatani, J. Miltat, and Y. Suzuki, Europhys. Lett. **69**, 990 (2005).
[4] T. Koyama, D. Chiba, K. Ueda, K. Kondou, H. Tanigawa, S. Fukami, T. Suzuki, N. Ohshima, N. Ishiwata, Y. Nakatani, K. Kobayashi, and T. Ono, Nat. Mater. **10**, 194 (2011).
[5] S. Zhang and Z. Li, Phys. Rev. Lett. **93**, 127204 (2004).
[6] G. Tatara, T. Takayama, H. Kohno, J. Shibata, Y. Nakatani, and H. Fukuyama, J. Phys. Soc. Jpn. **75**, 064708 (2006).
[7] M. Yan, A. Kákay, S. Gliga, and R. Hertel, Phys. Rev. Lett. **104**, 057201 (2010).
[8] O. Boulle, G. Malinowski, and M. Kläui, Mater. Sci. Eng. R **72**, 159 (2011).
[9] S. Lepadatu, J. S. Claydon, C. J. Kinane, T. R. Charlton, S. Langridge, A. Potenza, S. S. Dhesi, P. S. Keatley, R. J. Hicken, B. J. Hickey, and C. H. Marrows, Phys. Rev. B **81**, 020413 (2010).
[10] S. Lepadatu, J. Claydon, D. Ciudad, A. Naylor, C. Kinane, S. Langridge, S. Dhesi, and C. Marrows, Appl. Phys. Express **3**, 083002 (2010).
[11] I. M. Miron, G. Gaudin, S. Auffret, B. Rodmacq, A. Schuhl, S. Pizzini, J. Vogel, and P. Gambardella, Nat. Mater. **9**, 230 (2010).
[12] I. M. Miron, T. Moore, H. Szambolics, L. D. Buda-Prejbeanu, S. Auffret, B. Rodmacq, S. Pizzini, J. Vogel, M. Bonfim, A. Schuhl, and G. Gaudin, Nat. Mater. **10**, 419 (2011).
[13] K. Obata and G. Tatara, Phys. Rev. B **77**, 214429 (2008).
[14] A. Manchon and S. Zhang, Phys. Rev. B **79**, 094422 (2009).
[15] S. Emori, U. Bauer, S.-M. Ahn, E. Martinez, and G. S. D. Beach, Nat. Mater. **12**, 611 (2013).
[16] K.-S. Ryu, L. Thomas, S.-H. Yang, and S. Parkin, Nat. Nanotechnol. **8**, 527 (2013).
[17] F. Garcia-Sanchez, A. Kákay, R. Hertel, and P. Asselin, Appl. Phys. Express **4**, 033001 (2011).
[18] P. Grünberg, R. Schreiber, Y. Pang, M. B. Brodsky, and H. Sowers, Phys. Rev. Lett. **57**, 2442 (1986).
[19] C. Tsang, M. Pinarbasi, H. Santini, E. Marinero, P. Arnett, R. Olson, R. Hsiao, M. Williams, R. Payne, R. Wang, J. Moore, B. Gurney, T. Lin, and R. Fontana, IEEE Trans. Magn. **35**, 689 (1999).
[20] G. Tatara, H. Kohno, and J. Shibata, Phys. Rep. **468**, 213 (2008).
[21] A. Yamaguchi, K. Yano, H. Tanigawa, S. Kasai, and T. Ono, Jpn. J. Appl. Phys. **45**, 3850 (2006).
[22] N. L. Schryer and L. R. Walker, J. Appl. Phys. **45**, 5406 (1974).
[23] A. Hubert and R. Schäfer, *Magnetic Domains* (Springer-Verlag, Berlin, 2000).